MEDIUM VOLTAGE FAULT LOCATION USING DISTRIBUTED LV MEASUREMENTS

P. Bountouris*, H. Guo*, I. Abdulhadi*, F. Coffele*

**Power Networks Demonstration Centre, UK, panagiotis.bountouris@strath.ac.uk*

Keywords: MV fault location, distribution system, LV measurements, sequence components.

Abstract

An MV fault location technique based exclusively on low voltage measurements in the distribution network is presented in this paper. The technique is based on sequence component analysis of the voltage measurements in order to characterise the LV voltage during MV faults. The accuracy of the technique is evaluated using a DigSILENT PowerFactory model where various fault conditions have been studied including the impact of distributed generation connection on the network voltage profile. The model represents the Power Networks Demonstration Centre's (PNDC) MV and LV test network. This is to facilitate the validation of the model in the future implementing physical fault testing and measurements using the PNDC network.

1 Introduction

Accurate fault location is an important function in the toolkit of distribution system operators (DNOs) to ensure high level of supply availability. DNOs are incentivised to rapidly locate, isolate and repair fault to ensure Customer Minutes Lost (CI) and Customer Interruptions (CI) are minimised. [1].

Fault location can be challenging in distribution networks, particularly in the presence of distributed generation (DG) and during high impedance faults. Over the years academia and industry proposed a number of techniques to address some of the distribution network specific challenges of fault location [2] :

- Impedance based location (fundamental frequency).
- Travelling wave (high frequency transient analysis).
- Time Domain Reflectometry (TDR).
- Artificial Intelligence (knowledge based systems).
- Distributed measurements (e.g. smart meters, FPIs).

One of the most common techniques is based on the estimation of the apparent impedance to fault derived from the fundamental frequency voltage and current measurements. Those measurements are performed at single or multiple ends of the circuit [1], [3], [4]. Improved fault location accuracy can be achieved using multi end measurements, however this costs more due to the need for multiple measurement devices. Impedance based methods assume knowledge of the circuit impedance.

Travelling wave based fault location relies on the estimation of the time of arrival of high frequency signals originating from the point of fault inception on the circuit. The accuracy of this method can deteriorate in distribution networks depending on the presence of spurs and loading conditions. Furthermore, costly measurement equipment is required to perform the signal processing requires for this functionality [5], [6].

A less costly approach relies on Fault Passage Indicators (FPI) installed on the circuit which determine the passage of fault current and can send an alarm to the network operator to help in localising the fault. The presence of DG may necessitate directional FPIs (requiring voltage measurements) which increases the cost of deployment [5].

Low Voltage (LV) distribution networks are becoming increasingly instrumented, especially at secondary substations feeding customers. DNOs are increasingly deploying LV monitors to enhance the LV network observability [6]. A number of techniques focussing on fault location in radial circuits have been proposed. These rely on capturing fault induced voltage sag using distributed LV voltage measurements [7], [8].

This paper proposes a low cost fault location technique for MV networks (both radial and ring topology) based solely on LV voltage measurement, capitalising on the increasing presence of LV substation monitors and eliminates the need to install costly HV voltage and current sensors. The paper first presents the fault location principles, which are based on sequence component analysis. A simulation case study is then formulated and the results are then discussed with a view to further validate the technique in the future using physical testing at the PNDC [9].

2 Faulted Zone location technique

The proposed method is based on the distributed LV voltage measurements. The developed technique compares sequence components calculated during the fault to locate the MV Faulted Zone (FZ). An FZ would reside between MV pieces of switchgear to facilitate the isolation of the fault after its location.

The need to perform sequence component calculations dictates the technical requirements for the LV monitoring equipment

used. To derive the voltage sequence components, 3-phase voltage and phase angle are required. For LV monitoring, there are mainly two measurement locations. One is in the customer premises and the other is at the LV side of secondary substations [6] denoted as M1 – M6 in Figure 1. The devices in customer premises such as smart meters only obtain single phase quantities and it is not guaranteed that the smart meter will give the voltage measurement. On the other hand, the LV monitors in secondary substation generally measure 3-phase quantities including voltage, current, phase angles and power [6] and are thus the ideal data source for the proposed method. In addition, as the fault would be cleared within 0.1 s – 0.5 s [10], the LV monitors used for the proposed technique should also be able to measure the voltage RMS and angle values during the fault period. Modern LV monitors generally could record the waveform [11] [12] during the fault period and the waveform can then be used to derive both RMS and angle data.

The voltage magnitudes and angles are used to calculate the sequence components by the LV monitors, which in turn are used to calculate the following parameters: the ratio of positive over negative voltage sequence components (k_s, see eq. (1)) and the percentage difference of the ratios between different measurement points ($\Delta k_{s\%}$, see eq. (2)). The technique thus focuses on network imbalances caused by phase to ground, phase to phase and phase to phase to ground faults. Zero sequence components are not observed at the LV network during MV faults due to the delta/star connection of the MV/LV transformers.

The proposed fault location technique involves the use of a 'measuring window' of three adjacent LV monitoring points, referred as the 3-points window. The adjacency is from the point of view of the MV circuit (e.g. the LV monitoring point M2 is adjacent to M1). The window would calculate the positive sequence voltage (V_1) and negative sequence voltage (V_2) as well as k_s and $\Delta k_{s\%}$ at M1, M2 and M3. It is then moved downstream by one measurement point (i.e. M2, M3 and M4) and the process is repeated until the end of the circuit. For ring circuits, the final window location would return to include the first measurement point (i.e. M5, M6 and M1).

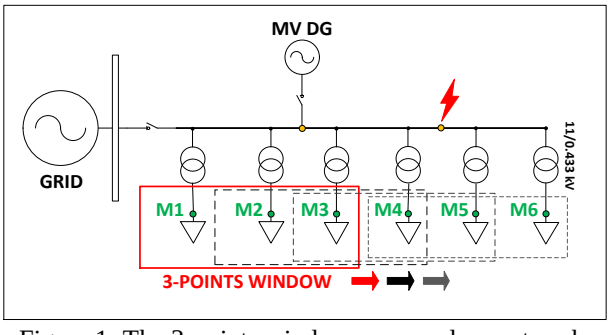

Figure 1: The 3-points window on a random network.

Equation (1) gives the ratio k_s, which could be described as a "balance factor" of the system as the higher the ratio the less imbalance prevails on the network. The positive over negative sequence voltage ratio:

$$k_s = \frac{V_1}{V_2} \quad (1)$$

Equation (2) calculates the percentage difference between the ratio k_s at various measurement points within a measurement window, where $\Delta k_{s_{ij}}$ is the difference between ratio k_{s_i} at point i and k_{s_j} at point j, whilst $\frac{\Sigma k_{s_{ij}}}{2}$ is the average value of factor k_{s_i} and k_{s_j}. It is applied to estimate the percentage differences between the adjacent nodes, $k_{s1} - k_{s2}$ and $k_{s2} - k_{s3}$, and the remote nodes, $k_{s1} - k_{s3}$, in a 3-points window.

$$\Delta k_{s_{ij\%}} = \frac{\Delta k_{s_{ij}}}{\frac{\Sigma k_{s_{ij}}}{2}} \times 100\% \quad (2)$$

3 Case study

3.1 Representation of PNDC network.

Power Networks Demonstration Centre (PNDC) is a research and demonstration facility, part of the University of Strathclyde, containing an 11 kV and LV configurable network [9]. The ultimate future goal of this study is to validate the proposed fault location method under real network conditions. For this purpose, modelling the PNDC network constitutes a critical task of the experiment, as the conducted investigation is planned to be demonstrated, by physical testing in PNDC facilities. In addition, the aforementioned developed models are established as base models, which can be further expanded to more complex configurations, thus more challenging scenarios.

Part of the modelling process was to build individually the PNDC network's components, according to the provided datasheets and related documentation. The main equipment including the Motor Generator (MG) Set, the isolation transformer 11/11 kV, the mock impedances (listed at Table 1) – which represent the overhead lines and underground cables – the step-down transformers 11/0.433 kV and the LV loads are depicted in Figure 2.

Mock impedance	*Resistance (Ω)*	*Inductance (mH)*
MI_1	0.16	0.6175
MI_2	0.16	0.6175
MI_3	0.016	0.062
MI_4	0.016	0.062
MI_5	0.032	0.124
MI_6	1.015	4.98
MI_7	1.015	4.98
MI_8	0.032	0.1241
MI_9	0.032	0.1241
MI_A	0.117	0.13
MI_B	0.117	0.13

MI_D	0.117	0.13
MI_E	0.117	0.13
MI_F	0.117	0.13

Table 1: Mock impedances.

The modelling has been done in the DigSILENT Power Factory software. Two base configurations are the radial and ring topologies without distributed generators, which represent the actual PNDC network. Both configurations are depicted in Figure 2.

An important part of the modelling process to enhance the study and increase the number of different scenarios is the development of alternative configurations in addition to the base configurations. The additional topologies involve connection of one distributed generator at the MV side or at the LV side, in both radial and ring topologies. **Error! Reference source not found.**2 below illustrates the DG connection points in both radial and ring topologies.

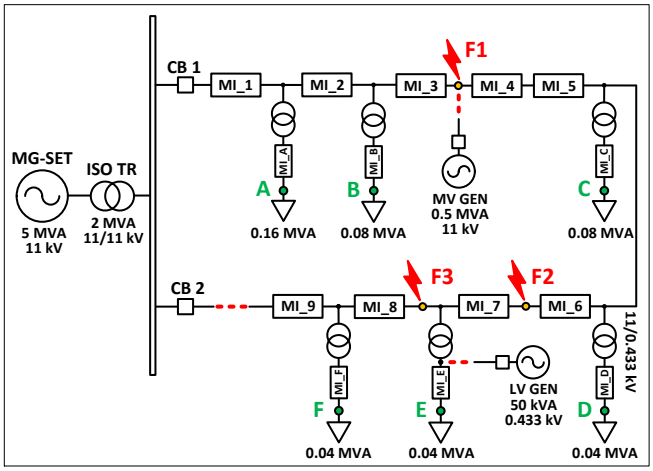

Figure 2: Representation of network including all base and alternative configurations along with all possible events.

The generator connected to the MV (11 kV) feeder is a 500kVA synchronous machine. The second generator, connected at the LV side of transformer E, is a synchronous machine with capacity of 50 kVA, nominal voltage 433 V and power factor (pf) 0.8. The reason of involving such a scenario is to investigate DG's impact on the LV voltage behaviour of the system – especially at the measurement point E – under several fault conditions.

3.2 Simulation cases

Key role on conducting an experiment of conclusive power is the variety and population of independent variables. The term "independent variables" refers to any changeable characteristic in the model. On the other hand, the output of dependent variables could be altered by changeable characteristic and these output values are examined. Manipulating the independent variables and simultaneously studying the effect of them on the dependent variables is a typical way for the experimenter to reach strong conclusions [13].

For this purpose, several scenarios combined different aspects of the model configuration with changes in the main parameters of the network components. For each of the configurations referred in previous section, different fault types at various locations were applied.

The LV voltage profile during both solid and resistive phase to ground and phase to phase faults, in three different locations, has been observed. For the real PNDC network, 20 Ω and 60 Ω is the minimum configurable fault resistance for the phase to ground and phase to phase fault, correspondingly. Hence, these two values were used in simulation in order to match the real PNDC network configurations. Table 2 below lists all the simulation cases.

Network configuration	*Fault locations*			*Fault types*			
				ph - ground		*ph - ph*	
Radial No DG	F1	F2	F3	0 Ω	20 Ω	0 Ω	60 Ω
Ring No DG	F1	F2	F3	0 Ω	20 Ω	0 Ω	60 Ω
Radial LV/ DG	F1	F2	F3	0 Ω	20 Ω	0 Ω	60 Ω
Ring LV/ DG	F1	F2	F3	0 Ω	20 Ω	0 Ω	60 Ω
Radial MV/DG	F1	F2	F3	0 Ω	20 Ω	0 Ω	60 Ω
Ring MV/DG	F1	F2	F3	0 Ω	20 Ω	0 Ω	60 Ω
Radial No DG	F1	F2	F3	0 Ω	20 Ω	0 Ω	60 Ω
Ring No DG	F1	F2	F3	0 Ω	20 Ω	0 Ω	60 Ω

Table 2: List of simulation cases.

Furthermore, the dependent variables of this study are taken into account for each of the above simulation cases. The group of those variables comprises of voltage root mean square (RMS), phase angle and sequence components captured from measurement units placed at the LV side of the transformers A, B, C, D, E and F, as indicated in Figure 2.

5 Results

In this section, the voltage sequence components data, extracted from simulations, are used to evaluate the proposed FZ location method. Due to lack of space, only the results produced by two fault types are going to be analysed for both radial and ring configuration.

5.1 Radial network

As discussed in section 2, the percentage differences, $\Delta k_{sij\%}$, captured by the 3-points window, is a key element for the location of a faulted zone. In Table , all $\Delta k_{s13\%}$ data aroused after a phase to ground fault (20 Ω) are listed for each scenario. The results show that the 3-points window with the maximum $\Delta k_{s13\%}$ in the network contains the corresponding fault zone.

The highlighted values in Table prove that the above statement is a fact for all the simulation cases, under the particular fault type. For example, in scenarios where fault occurs at F1 (see Figure 2), the greatest percentage difference is the $\Delta k_{sAC\%}$ and this implies the correct fault zone, A-B-C.

DG	*Fault location*	$\Delta k_{s_{AC}}$ (%)	$\Delta k_{s_{BD}}$ (%)	$\Delta k_{s_{CE}}$ (%)	$\Delta k_{s_{DF}}$ (%)
No	F1	2.56	0.23	$4e^{-5}$	$1e^{-5}$
	F2	3.25	1.16	16.89	17.62
	F3	3.24	1.16	30.92	34.60
MV	F1	2.47	0.22	$1e^{-4}$	$3e^{-4}$
	F2	3.28	1.31	19.55	20.59
	F3	3.28	1.31	35.28	40.10
LV	F1	2.53	0.22	-22.68	-0.63
	F2	3.23	1.15	-4.63	15.94
	F3	3.22	1.15	10.63	32.06

Table 3: 3-points window percentage differences, $\Delta k_{s13\%}$, for ph-ground resistive (20 Ω) fault.

Similarly, the $\Delta k_{s13\%}$ results after a phase to phase (ph-ph) fault (60 Ω), listed in the Table 4, indicate the fault zone accurately.

DG	*Fault location*	$\Delta k_{s_{AC}}$ (%)	$\Delta k_{s_{BD}}$ (%)	$\Delta k_{s_{CE}}$ (%)	$\Delta k_{s_{DF}}$ (%)
No	F1	2.66	0.23	$6e^{-5}$	$13e^{-5}$
	F2	3.37	1.21	17.47	18.26
	F3	3.37	1.21	31.97	35.93
MV	F1	2.55	0.22	$1e^{-4}$	$1e^{-4}$
	F2	3.38	1.36	20.11	21.21
	F3	3.38	1.35	36.28	41.41
LV	F1	2.63	0.21	-22.84	-0.65
	F2	3.35	1.20	-4.25	16.50
	F3	3.34	1.20	11.47	33.24

Table 4: 3-points window percentage differences, $\Delta k_{s13\%}$, for ph-ph resistive (60 Ω) fault.

Solid ph-g and ph-ph faults were also applied with the same level of success.

5.2 Ring network

In this section, the results related to the ring configurations study are listed in Table 1. A comparative analysis to the derived sequence components ratios, k_s, is applied. The proposed method uses the indexes '1' and '0' as the outcome of the comparison between two adjacent measurement points. For example, if k_s at point A is greater than this at point B then the index will be '1'. In other case, the index is '0'. The moving 3-points window tracks all the resulted indexes across the network and records any change from '1' to '0'. If only one change from '1' to '0' occurs, the corresponding 3-point window contains the fault zone. For instance, when a fault (ph-g 20 Ω) occurs at F1, B>C is '1' whilst C>D is '0'. Therefore, the fault zone is in the window B-C-D (see Table 5).

When more than one changes from '1' to '0' exist, the selection of the 3-points window with the highest value of either $|\Delta k_{s12\%}|$ or $|\Delta k_{s23\%}|$ needs to be examined.

DG	*Fault location*	*Sequence components ratio, k_s comparisons indexes*					
		A>B	*B>C*	*C>D*	*D>E*	*E>F*	*F>A*
No	F1	1	1 ⇢ 0	0	0	0	1
	F2	1	1	1 ⇢ 0	0	0	1
	F3	1	1	1	1 ⇢ 0	0	0
MV	F1	1	1 ⇢ 0	0	0	0	1
	F2	1	1	1 ⇢ 0	0	0	1
	F3	0	1	1	1 ⇢ 0	0	0
LV	F1	1	1 ⇢ 0	0	0	1	1
	F2	1	1	1 ⇢ 0	0	1	1
	F3	1	1	1 ⇢ 0	0	1 ⇢ 0	

Table 1: Ring configuration sequence components ratios comparisons, for ph-g resistive (20 Ω) fault.

Relevant data taken during a particular scenario, with the presence of an LV DG in the network and under resistive fault (20 Ω) conditions, have been collected and listed in Table 2 below. Both 3-points windows C-D-E and E-F-A showed changes form '1' to '0' so, their $|\Delta k_{s12\%}|$ and $|\Delta k_{s23\%}|$ have to be compared.

DG	*Fault location*	$\lvert\Delta k_{s_{CD}}\rvert$ (%)	$\lvert\Delta k_{s_{DE}}\rvert$ (%)	$\lvert\Delta k_{s_{EF}}\rvert$ (%)	$\lvert\Delta k_{s_{FA}}\rvert$ (%)
LV	F3	0.005	19.22	19.55	0.41

Table 2: Absolute values of percentage differences, $|\Delta k_{s12\%}|$ and $|\Delta k_{s23\%|}$, for ph-g resistive (20 Ω) fault.

The highlighted cell in Table 2 contains the highest value, $|\Delta k_{sEF\%}|$, which belongs to the 3-points window E-F-A. Consequently, the fault zone is located within the area E-F-A.

DG	*Fault location*	*Sequence components ratio, k_s comparisons indexes*					
		A>B	*B>C*	*C>D*	*D>E*	*E>F*	*F>A*
No	F1	1	1 ⇢ 0	0	0	0	1
	F2	1	1	1 ⇢ 0	0	0	1
	F3	1	1	1	1 ⇢ 0	0	0
MV	F1	1	1 ⇢ 0	0	0	0	1
	F2	1	1	1 ⇢ 0	0	0	1

	F3	0	1	1	1 ⇢ 0	0
LV	F1	1	1 ⇢ 0	0	1	1
	F2	1	1	1 ⇢ 0	1	1
	F3	1	1	1 ⇢ 0	1 ⇢ 0	

Table 7: Ring configuration sequence components ratios comparisons, for ph-ph resistive (60 Ω) fault.

As it can be seen in Table 7, the relevant comparisons results aroused under ph-ph 60 Ω fault are exactly the same with those under ph-g 20 Ω. Similarly with the previous case, the corresponding scenario, including the LV DG connection and F3 fault location, presents two 3-points windows with changes from '1' to '0'. Table 8 below contains the $|\Delta k_{s12\%}|$ and $|\Delta k_{s23\%}|$ data under investigation, in an attempt to identify the FZ. The highlighted value is the highest among the others and belongs to the E-F-A 3-points window, indicating the FZ.

DG	*Fault location*	$\lvert\Delta k_{s_{CD}}\rvert$ (%)	$\lvert\Delta k_{s_{DE}}\rvert$ (%)	$\lvert\Delta k_{s_{EF}}\rvert$ (%)	$\lvert\Delta k_{s_{FA}}\rvert$ (%)
LV	F3	0.01	19.29	19.63	0.43

Table 8: Absolute values of percentage differences, $|\Delta k_{s12\%}|$ and $|\Delta k_{s23\%}|$, for ph-ph resistive (60 Ω) fault.

Figure 3 represents graphically the '1' and '0' record across the ring network. Changes from '0' to '1' give a "positive" peak in this diagram and denote the presence of at least one generator, which is able to support the voltage at the LV side of the transformers. On the other hand, the "negative" peaks are introduced by the '1' to '0' changes and reveal the presence of faults. The particular scheme describes how the DG connected at the LV side of transformer E and the main 5 MVA generator as well as the fault F3 contribute to the deviation of the ratio k_s across the network.

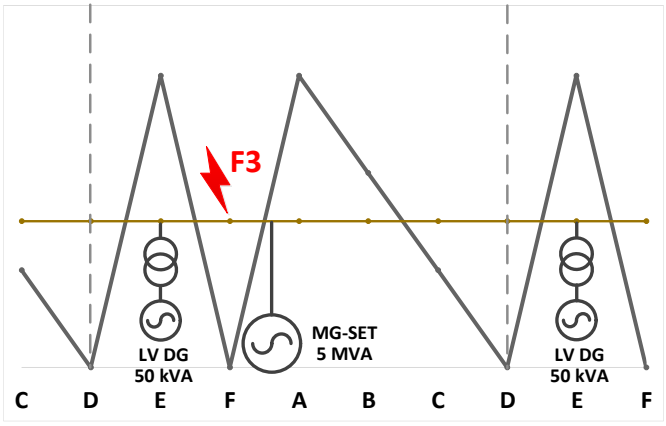

Figure 3: Graphical representation of comparative analysis indexes record. The F3 (ph-g 20 Ω) occurs on a network with an LV DG connected at the LV side of transformer F.

Another example corresponding to the scenario with no DG connection and a ph-ph fault (60 Ω) injected between transformers B and C is demonstrated in Figure 4, below.

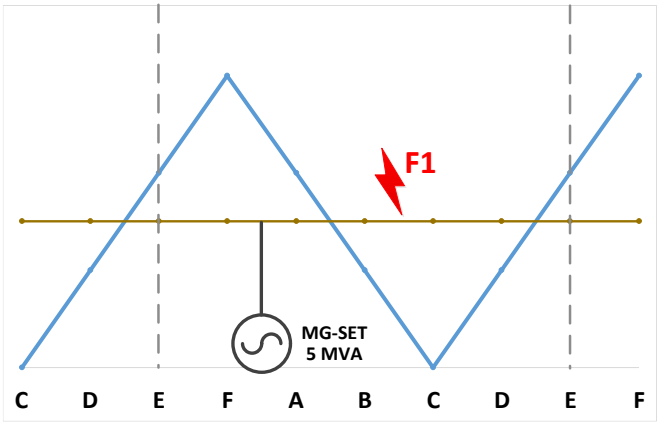

Figure 4: Graphical representation of comparative analysis indexes record. The F1 occurs in a ring network with no any DG connected.

6 Conclusions

The paper proposed the use of LV substation monitors as a cost effective means of identifying the fault location in an 11kV network. A study based on a DIgSILENT PowerFactory model of the PNDC has been used to characterise the LV voltage profile and sequence components during an MV fault. The simulation results indicate a distinct pattern of measured parameters which can be used to accurately locate the MV fault location between adjacent LV voltage monitoring locations. This would facilitate the rapid location of MV faults and aid in the restoration of customer supplies.

It is worth noting, however, that certain requirements need to be satisfied so that the fault location can be reliably achieved:

- Accurate voltage RMS and angle measurements are required for the correct calculation of the sequence components.
- Calibration and coordination of the metering units with the aid of telecommunication systems is a prerequisite for the normal operation of the fault location technique. However, the communications system requirements should not be onerous due to the minimal amount of information that needs to be transferred for the comparison between LV measurement locations.

It is envisaged that an implementation of an algorithm, based on the identified LV voltage profile characteristics, will be deployed in the PNDC test network and validated using physical testing.

Acknowledgements

The funding provided for this research work by PNDC's industrial membership through the Core Research Programme is gratefully acknowledged.

References

[1] F. M. Aboshady, M. Sumner, and D. W. P. Thomas, "A double end fault location technique for distribution systems based on fault-generated transients," in *2017 IEEE 26th International Symposium on Industrial Electronics (ISIE)*, 2017, pp. 32–36.

[2] J. Cordova and M. O. Faruque, "Fault location identification in smart distribution networks with Distributed Generation," in *2015 North American Power Symposium (NAPS)*, 2015, pp. 1–7.

[3] R. Krishnathevar and E. E. Ngu, "Generalized Impedance-Based Fault Location for Distribution Systems," *IEEE Trans. Power Deliv.*, vol. 27, no. 1, pp. 449–451, Jan. 2012.

[4] F. M. Abo-Shady, M. A. Alaam, and A. M. Azmy, "Impedance-based fault location technique for distribution systems in presence of distributed generation," in *2013 IEEE International Conference on Smart Energy Grid Engineering (SEGE)*, 2013, pp. 1–6.

[5] J. Altonen and A. Wahlroos, "Performance of modern fault passage indicator concept in compensated MV-networks," in *CIRED Workshop 2016*, 2016, pp. 1–4.

[6] Mike Lees (EA Technology Limited), "Enhanced Network Monitoring Report," 2014.

[7] R. A. F. Pereira, L. G. W. da Silva, M. Kezunovic, and J. R. S. Mantovani, "Improved Fault Location on Distribution Feeders Based on Matching During-Fault Voltage Sags," *IEEE Trans. Power Deliv.*, vol. 24, no. 2, pp. 852–862, Apr. 2009.

[8] A. Teninge, C. Pajot, B. Raison, and D. Picault, "Voltage profile analysis for fault distance estimation in distribution network," in *2015 IEEE Eindhoven PowerTech*, 2015, pp. 1–5.

[9] C. D. Booth, F. Coffele, and G. M. Burt, "The Power Networks Demonstration Centre: An environment for accelerated testing, demonstration and validation of existing and novel protection and automation systems," in *12th IET International Conference on Developments in Power System Protection (DPSP 2014)*, 2014, pp. 1–6.

[10] N. F. Sherbilla, T. A. Kawady, N. I. Elkalashy, and A. M. I. Taalab, "Modified setting of overcurrent protection for distribution feeders with distributed generation," in *IET Conference on Renewable Power Generation (RPG 2011)*, 2011, pp. 1–6.

[11] Embedded Monitoring System, "sub.net Substation Monitoring Simplified," 2011.

[12] Beckhoff, "EL3773 Power Monitoring Oversampling Terminal," 2017.

[13] "Independent and Dependent Variables," *Statistics Solutions*, 03-Feb-2010. .